

This is a revised version of an article submitted for consideration in Acta Materialia (copyright Elsevier). Acta Materialia is available online at:
<http://www.journals.elsevier.com/acta-materialia>

ON "MACROSCOPIC" CHARACTERIZATION OF MIXED GRAIN BOUNDARIES

A.Morawiec* and K.Glowinski

Polish Academy of Sciences, Institute of Metallurgy and Materials Science

Reymonta 25, 30-059 Kraków, Poland

(*) E-mail: nmmorawi@cyf-kr.edu.pl

Tel.: ++48-122952854 Fax: ++48-122952804

Abstract: Grain boundaries having no special geometric features are referred to as mixed. Mixed boundaries constitute a large class, and the need for a finer differentiation arises. A mixed boundary can be characterized by linking it to the nearest boundaries with special geometric attributes, in particular, by its decomposition into twist and tilt components. We investigate and compare the quantitative methods and parameters used for description of mixed boundaries. The considered methods are based either on the decomposition or on some other measures of deviations from pure-twist or pure-tilt boundaries. Furthermore, the methods are either limited to boundary representations with the smallest misorientation angles or take into account all symmetrically equivalent boundary representations, and these two approaches differ in their meaning, physical significance and conclusions. The relationships between the methods of mixed boundary characterization are clarified and the suitability of particular parameters for analysis of experimental data is assessed. These issues are important for a thorough understanding of grain boundary distributions in the space of macroscopic boundary parameters. The considered techniques and parameters are used to examine mixed boundaries in Ni-based superalloy IN100.

Keywords: Grain boundary; Microstructure; Misorientation; Macroscopic boundary parameters; Nickel alloys

1. Introduction

Properties of polycrystals are known to be influenced by grain boundaries [1]. A complete description of structures of grain boundary networks is beyond current experimental capabilities, but grain misorientations and vectors locally normal to boundaries, i.e., the so-called "macroscopic boundary parameters" [2], are accessible. Grain misorientations are routinely measured via acquisition of orientation maps, and there is also a considerable progress in research involving both misorientations and boundary inclinations. Moreover, conventional experiments on bicrystals are being supplemented by measurements on sectioned polycrystals (e.g., [3]) and by tomographic techniques (e.g., [4]). These new methods provide boundary data sets sufficiently large for performing statistical analyzes of boundaries.

To grasp the vast (five dimensional) boundary space, some classifications and reference boundaries are needed. Besides the partition into small- and large-angle boundaries and the assignment of a CSL number, which take into account only grain misorientations, it is common to describe boundaries as twist or tilt. With \mathbf{n} denoting a unit vector ($\mathbf{n} \cdot \mathbf{n} = \mathbf{n}^2 = 1$) normal to the boundary plane and \mathbf{u} being a unit vector along the misorientation axis, a boundary is referred to as twist or tilt if it has a representation such that $|\mathbf{n} \cdot \mathbf{u}|$ equals 1 or 0, respectively. In other words, a twist boundary has a representation with the misorientation axis perpendicular to the boundary plane, and a tilt boundary has a representation with the axis in this plane. Low-index twist and tilt boundaries can be relatively easily visualized, and – more importantly – they frequently serve as a proving ground for various grain boundary analyzes (e.g., [5, 6]).

Ideal (pure) twist and tilt boundaries are special cases. Most boundaries are neither twist nor tilt; they are referred to as mixed. Despite the size of the class of mixed boundaries, in many studies, they are eclipsed by the geometrically special cases. Therefore, in analysis of error-affected experimental data, the need for a finer characterization of mixed boundaries arises. For that, some quantitative parameters are needed, and one standardly refers to the notions of twist and tilt 'components' of mixed boundaries. The concept of 'de-composition' of boundaries into twist and tilt components is discussed in most introductions to grain boundaries (e.g., [1, 7]). However, the literature is frequently vague about the decomposition of symmetrically equivalent boundary representations and about expected end-results of the decomposition. Moreover, it completely ignores practical aspects of application of the decomposition to analysis of error-affected boundary data.

Below, we explore ways of quantitative characterization of mixed boundaries. In particular, we analyze in detail their decomposition. Because of symmetry, the decomposition leads to multiple results, and the basic question is, what should be accepted as a quantitative outcome of the procedure. There are also the related problems of the meaning of

particular results, and the relevance of the angles of twist and tilt components as measures of the closeness of a boundary to the twist or tilt geometry. Some of these issues have been raised before (e.g., [1, 8–10]), but none of the previous accounts is complete. Besides the angles of components, there are other parameters linking mixed boundaries with twists and tilts. One pair of parameters is based on properly defined distances of mixed boundaries to the nearest pure-twist and pure-tilt boundaries, and another uses the parameter $|\mathbf{n} \cdot \mathbf{u}|$ and its extrema over equivalent boundary representations.

These approaches to quantitative analysis of mixed boundaries are described and compared. A distinction must be made between methods using just boundary representations with the smallest misorientation angles and those using all equivalent boundary representations. They give very different depictions of distributions of particular boundary types. Within the class of approaches taking into account equivalent representations the differences are small, but they have an impact on practical applicability of particular parameters to analysis of experimental data.

We begin by introducing notation and basic mathematical aspects of grain boundary decomposition. Next, the impact of symmetries is examined; with crystal symmetry taken into account, the decomposition becomes ambiguous (“degenerate” in parlance of [8]), and we consider distinctness of its results. Then, the decomposition is confronted with other ways of quantifying the degree of tilt and twist. Finally, we use the considered parameters to investigate mixed boundaries in the Ni-based superalloy IN100.

For simplicity, our considerations are confined to centrosymmetric crystals. This allows for limiting the needed symmetries to proper rotations of crystal point group. For convenience, the final sections and all our examples are limited to the cubic $m\bar{3}m$ (O_h) crystal symmetry.

2. Notation

Of all texts concerning the boundary decomposition, the article of Fortes [9] seems to be closest to our considerations, and the notation used below stems from that paper. Differently than in [9], rotations are parametrized by Rodrigues vectors. This parametrization simplifies some derivations and expressions. It was already used for describing boundary decomposition in [1] (p.23), but that account is enigmatic and incomplete.

Calculations utilizing the Rodrigues parameterization are particularly easily performed in Cartesian reference systems linked to crystal structures. In this parameterization, a rotation about \mathbf{u} by the angle θ ($0^\circ \leq \theta \leq 180^\circ$) corresponds to the vector $\mathbf{U} = \tan(\theta/2)\mathbf{u}$. Hence, the rotation inverse to \mathbf{U} corresponds to $-\mathbf{U}$, and the identity corresponds to the vector of zero magnitude which will be denoted by $\mathbf{0}$. The rotation $\mathbf{N} \circ \mathbf{L}$ being a composition

of rotations \mathbf{N} and \mathbf{L} is given by

$$\mathbf{N} \circ \mathbf{L} = (\mathbf{N} + \mathbf{L} - \mathbf{N} \times \mathbf{L}) / (1 - \mathbf{N} \cdot \mathbf{L}) .$$

Formally, the product "o" can also be applied to arbitrary vectors not representing rotations. In particular, a vector, say \mathbf{v} , after rotation represented by \mathbf{U} becomes $\mathbf{U} \circ \mathbf{v} \circ (-\mathbf{U})$. For more detailed introduction to Rodrigues parameters and conventions used see [11].

Within the macroscopic description, a planar segment of a boundary of a grain is determined by the pair (\mathbf{U}, \mathbf{n}) , where \mathbf{n} is a unit outward normal and \mathbf{U} represents misorientation of a neighboring grain. We use the convention with the left side of \mathbf{U} linked to the coordinate system in which \mathbf{n} is given. If the same boundary is expressed in the system of the other grain, the misorientation corresponds to the vector $\mathbf{U}' = -\mathbf{U}$, and the boundary normal is $\mathbf{n}' = -((-\mathbf{U}) \circ \mathbf{n} \circ \mathbf{U})$.

3. Twist and tilt components

Briefly, the twist (\mathbf{N}) and tilt (\mathbf{L}) components of the grain misorientation \mathbf{U} with respect to the boundary normal \mathbf{n} are parts of the factorization of \mathbf{U} into a product of \mathbf{N} and \mathbf{L} , where \mathbf{N} represents a rotation about \mathbf{n} , and \mathbf{L} is a rotation about an axis perpendicular to \mathbf{n} [8,9]. More precisely, for given finite \mathbf{U} ($\neq \mathbf{0}$) and unit normal \mathbf{n} , the twist \mathbf{N} and tilt \mathbf{L}_1 satisfying the requirements $\mathbf{U} = \mathbf{N} \circ \mathbf{L}_1$, $\mathbf{N} \propto \mathbf{n}$ and $\mathbf{N} \cdot \mathbf{L}_1 = 0$, have the forms

$$\mathbf{N} = (\mathbf{U} \cdot \mathbf{n}) \mathbf{n} \quad \text{and} \quad \mathbf{L}_1 = (-\mathbf{U} \cdot \mathbf{n}) \mathbf{n} \circ \mathbf{U} . \quad (1)$$

Analogously, $\mathbf{U} = \mathbf{L}_2 \circ \mathbf{N}$ together with $\mathbf{N} \propto \mathbf{n}$ and $\mathbf{N} \cdot \mathbf{L}_2 = 0$ leads to

$$\mathbf{N} = (\mathbf{U} \cdot \mathbf{n}) \mathbf{n} \quad \text{and} \quad \mathbf{L}_2 = \mathbf{U} \circ (-\mathbf{U} \cdot \mathbf{n}) \mathbf{n} . \quad (2)$$

If \mathbf{U} is a half-turn (180° -rotation) and $\mathbf{n} \cdot \mathbf{u} \neq 0$, then \mathbf{N} is a half-turn, and $\mathbf{L}_1 = \mathbf{n} \times \mathbf{u} / (\mathbf{n} \cdot \mathbf{u}) = -\mathbf{L}_2$. If \mathbf{U} is a half-turn and $\mathbf{n} \cdot \mathbf{u} = 0$, there are infinite number of solutions with tilts being half-turns about arbitrary axes perpendicular to \mathbf{n} and twists being rotations by twice the angles between tilt axes and \mathbf{u} ; further on, this particular case is neglected.

The twist component \mathbf{N} is the same in both types ($\mathbf{N} \circ \mathbf{L}_1$ and $\mathbf{L}_2 \circ \mathbf{N}$) of the decomposition. The vectors \mathbf{L}_1 and \mathbf{L}_2 are generally different, but they have equal magnitudes. If \mathbf{L}_i is non-zero, it can be expressed as $\mathbf{L}_i = (\mathbf{U} \cdot \mathbf{l}_i) \mathbf{l}_i$, where the unit vector \mathbf{l}_i is obtained by normalization of \mathbf{L}_i . Thus, the respective angles ν and λ of the rotations \mathbf{N} and \mathbf{L}_i are given by

$$\tan(\nu/2) = \sqrt{\mathbf{N}^2} = |\mathbf{U} \cdot \mathbf{n}| \quad \text{and} \quad \tan(\lambda/2) = \sqrt{\mathbf{L}_i^2} = |\mathbf{U} \cdot \mathbf{l}_i| ,$$

where \mathbf{N}^2 and \mathbf{L}_i^2 denote $\mathbf{N} \cdot \mathbf{N}$ and $\mathbf{L}_i \cdot \mathbf{L}_i$, respectively. Since $\mathbf{N} \circ \mathbf{L}_1 = \mathbf{U} = \mathbf{L}_2 \circ \mathbf{N}$, the second of the two tilts can be expressed as $\mathbf{L}_2 = \mathbf{N} \circ \mathbf{L}_1 \circ (-\mathbf{N})$, i.e, the vector \mathbf{L}_2 equals to

\mathbf{L}_1 rotated by \mathbf{N} . If $\mathbf{L}_1 = \mathbf{L}_2$, then either $\mathbf{N} = \mathbf{0}$ or $\mathbf{L}_i = \mathbf{0}$. Clearly, if either \mathbf{N} or \mathbf{L}_i equals $\mathbf{0}$, the other one equals \mathbf{U} , and vice versa, if either of them equals \mathbf{U} , the other one is $\mathbf{0}$. Relationships between directions and magnitudes of \mathbf{U} , \mathbf{N} and \mathbf{L}_i are illustrated in Fig. 1. Fig. 1

For a given \mathbf{U} , the twist and tilt angles ν and λ as functions of \mathbf{n} are symmetric with respect to rotations about \mathbf{u} . In other words, the decomposition of \mathbf{U} with respect to \mathbf{n} gives the same angles as that with respect to $(\xi\mathbf{u}) \circ \mathbf{n} \circ (-\xi\mathbf{u})$, where ξ is an arbitrary real number. Similarly, for a given \mathbf{n} , the twist and tilt angles as functions of \mathbf{U} are symmetric with respect to rotations about \mathbf{n} ; the decomposition of \mathbf{U} with respect to \mathbf{n} gives the same angles as the decomposition of $(\xi\mathbf{n}) \circ \mathbf{U} \circ (-\xi\mathbf{n})$ with respect to the same vector \mathbf{n} . Moreover, from $\mathbf{N} \circ \mathbf{L}_1 = \mathbf{U} = \mathbf{L}_2 \circ \mathbf{N}$ under the condition $\mathbf{N} \cdot \mathbf{L}_i = 0$, one gets

$$1 + \mathbf{U}^2 = (1 + \mathbf{N}^2)(1 + \mathbf{L}_i^2) \quad (3)$$

(or, in terms of the angles, $\cos(\theta/2) = \cos(\nu/2) \cos(\lambda/2)$ [9]). This implies that the magnitudes of the components \mathbf{N} or \mathbf{L}_i cannot exceed the magnitude of \mathbf{U} . Consequently, neither the twist angle ν nor the tilt angle λ can exceed the misorientation angle θ . The tilt angle λ is additionally bounded from top by 2α , where $\alpha = \arccos(|\mathbf{n} \cdot \mathbf{u}|)$ is the angle between directions of \mathbf{n} and \mathbf{u} . Proofs of the above claims are given in Appendix.

4. Impact of symmetries

A boundary can be represented in an equivalent way by a number of different (\mathbf{U}, \mathbf{n}) pairs. The equivalences appear because of the crystal symmetry and the grain exchange symmetry [12]. The latter must be taken into account if grains cannot be identified in a unique way (as in experiments on polycrystals), and it means that (\mathbf{U}, \mathbf{n}) is equivalent to $(\mathbf{U}', \mathbf{n}')$. Because of crystal symmetry, the identification of a boundary by (\mathbf{U}, \mathbf{n}) is equivalent to those by $(\mathbf{U}, -\mathbf{n})$ and $(\mathbf{S}_L \circ \mathbf{U} \circ (-\mathbf{S}_R), \mathbf{S}_L \circ (\pm\mathbf{n}) \circ (-\mathbf{S}_L))$, where the Rodrigues vectors \mathbf{S}_L and \mathbf{S}_R represent proper rotations of the crystal point group [12]. We take into account all equivalent representations $\mathbf{S}_L \circ \mathbf{U} \circ (-\mathbf{S}_R)$ in accord with the current standards in analysis of grain misorientations [13–15]; in older papers, e.g. [9], only symmetry of one crystal is explicitly considered while that of the other crystal is tacitly assumed. With our focus on the cubic holohedry, \mathbf{S}_L and \mathbf{S}_R are elements of the 432 (O) point group.

There is a question about additional ambiguities of decomposition, other than the two tilt components \mathbf{L}_1 and \mathbf{L}_2 , arising from the equivalences. Let us first consider the exchange of the grains. The decomposition of $\mathbf{U}' = -\mathbf{U} = -((-\mathbf{U}) \circ \mathbf{U} \circ \mathbf{U})$ with respect to the normal $\mathbf{n}' = -((-\mathbf{U}) \circ \mathbf{n} \circ \mathbf{U})$ leads to twist and tilt components

$$\mathbf{N}' = -((-\mathbf{U}) \circ \mathbf{N} \circ \mathbf{U}), \quad \mathbf{L}'_1 = -((-\mathbf{U}) \circ \mathbf{L}_2 \circ \mathbf{U}) \quad \text{and} \quad \mathbf{L}'_2 = -((-\mathbf{U}) \circ \mathbf{L}_1 \circ \mathbf{U}).$$

Thus, the vectors \mathbf{N}' , \mathbf{L}'_1 and \mathbf{L}'_2 represent the same rotations as \mathbf{N} , \mathbf{L}_2 and \mathbf{L}_1 in a different coordinate system. In other words, the vectors resulting from the decompositions for the

equivalent pairs (\mathbf{U}, \mathbf{n}) and $(\mathbf{U}', \mathbf{n}')$ are congruent and are considered as identical, i.e., the exchange of grains does not lead to geometrically different results.

Let us now proceed to the impact of crystal symmetries. Based on eqs. (1) and (2), it is easy to see that neither \mathbf{N} nor \mathbf{L}_i depend on the sense of the vector \mathbf{n} , so the equivalence between (\mathbf{U}, \mathbf{n}) and $(\mathbf{U}, -\mathbf{n})$ is irrelevant for the decomposition. On the other hand, the decomposition of equivalent misorientations $\mathbf{S}_L \circ \mathbf{U} \circ (-\mathbf{S}_R)$ with respect to $\mathbf{S}_L \circ \mathbf{n} \circ (-\mathbf{S}_L)$ may give many numerically different results. However, since for the same symmetry operation \mathbf{S}_L on both sides of \mathbf{U} one has

$$\mathbf{S}_L \circ \mathbf{U} \circ (-\mathbf{S}_L) = \mathbf{S}_L \circ \mathbf{N} \circ \mathbf{L}_1 \circ (-\mathbf{S}_L) = (\mathbf{S}_L \circ \mathbf{N} \circ (-\mathbf{S}_L)) \circ (\mathbf{S}_L \circ \mathbf{L}_1 \circ (-\mathbf{S}_L)) ,$$

(plus similar relationship for $\mathbf{L}_2 \circ \mathbf{N}$), the decompositions of \mathbf{U} and $\mathbf{S}_L \circ \mathbf{U} \circ (-\mathbf{S}_L)$ lead to congruent results. Let $\mathbf{S}_L \circ (-\mathbf{S}_R) = \mathbf{S}$. For getting non-congruent decompositions of all equivalent representations $\mathbf{S}_L \circ \mathbf{U} \circ (-\mathbf{S}_R) = (\mathbf{S}_L \circ \mathbf{U} \circ (-\mathbf{S}_L)) \circ \mathbf{S}$, it is enough to consider the equivalence of \mathbf{U} and $\mathbf{U} \circ \mathbf{S}$ with the symmetry operation \mathbf{S} on just one side of \mathbf{U} . The operation \mathbf{S} was arranged to act on the right side, so the change of the representation from \mathbf{U} to $\mathbf{U} \circ \mathbf{S}$ has no impact on the boundary normal \mathbf{n} .

Despite numerous references to twist and tilt components of mixed boundaries, there are no definite guidelines on the 'end-product' of the decomposition. In general, with all the combinations involving \mathbf{L}_1 and \mathbf{L}_2 for each $\mathbf{U} \circ \mathbf{S}$, the decomposition leads to a compound result; in the cubic case, up to 48 different pairs of twist and tilt components may be ascribed to a mixed boundary. There is no simple prescription for, or purpose in dealing simultaneously with all these pairs. On the other hand, if only some of the results are to be selected, one needs criteria and physical, geometrical or computational reasons for the selection.

One of these criteria is simple and common. Instead of considering decompositions of all equivalent boundary representations, it is convenient to focus only on the representatives \mathbf{U} with the smallest misorientation angle (usually referred to as *disorientations* [8]), and to ignore symmetries other than $\mathbf{S} \circ \mathbf{U} \circ (-\mathbf{S})$. This leads to a unique (up to congruence) set of \mathbf{N} and \mathbf{L}_i vectors and to unique twist and tilt angles. A disorientation is sometimes additionally restricted by the requirement that the misorientation axis is in the 'standard triangle'. Since the angle preserving transformations $\mathbf{S} \circ \mathbf{U} \circ (-\mathbf{S})$ are linked to the transformations of the normal $\mathbf{S} \circ \mathbf{n} \circ (-\mathbf{S})$, this additional restriction has no impact on the results of decomposition.

5. Quantifying the degree of tilt or twist

The most basic objective of the decomposition is to infer how a boundary deviates from pure-tilt and pure-twist geometries. For that a "degree of tilt or twist at the boundary" [16] is needed. This degree can be measured by angles of the twist and tilt components, but

that is not the only way to put a figure on it. Below, we discuss and confront two different implementations of the decomposition and other approaches to quantification of tilts and twists in boundaries.

5.1 Decomposition of disorientations

It is easy and convenient to limit the decomposition to boundary representations based on disorientations. As was mentioned above, this leads to unique twist (ν) and tilt (λ) angles. Values of ν and λ can be ascribed to every planar segment of a boundary. The distributions of these angles are simple and smooth. They vary continuously with misorientation and plane parameters. Example sections through these distributions for the $\Sigma 7$ disorientation (38.2° rotation about the [111] axis) are shown in Fig. 2.

Fig. 2

This computationally convenient approach has a relevant negative aspect. Certain features of boundaries are not apparent when only the smallest-angle representations are considered, because to expose them, all symmetries need to be taken into account. The classic example of that is the coherent twin boundary in *fcc* metals. The decomposition of the particular (smallest-angle) representation $\mathbf{U} = (1, 1, 1)/3$ of the $\Sigma 3$ misorientation with respect to $\mathbf{n} = (1, 1, 1)/\sqrt{3}$ gives $\mathbf{N} = \mathbf{U}$ and $\mathbf{L}_i = \mathbf{0}$, i.e., the boundary is a pure twist. It is well-known, however, that this boundary can also be seen as a tilt boundary (see below). This property can be detected only by considering the representations with larger misorientation angles, i.e., it is not detectable within the scheme limited to disorientations. Similar considerations are applicable to other boundaries; for instance, almost all low- Σ twist boundaries have also tilt character [17, 18]. In order to get complete geometric specification of a boundary, all its representations need to be examined.

A more general argument against using disorientation is that its definition relies on one of the five macroscopic boundary parameters (the misorientation angle), and in the case of large-angle boundaries, there is no reason for distinguishing this particular parameter as having more significance than the other four parameters.

5.2 Fortes decomposition

To avoid drawbacks of the decomposition of disorientations, Fortes [9] proposed to check all boundary representations, and to "choose the description involving the smallest angle of tilt or twist, so as to make the boundary, as nearly as possible, a pure-twist or a pure-tilt boundary." It is shown below that this idea is applicable only to perfect error-free data.

We will denote the smallest possible twist and tilt angles by ν_F and λ_F , respectively. Clearly, the Fortes method reveals the pure-twist and pure-tilt boundaries. E.g., for the *fcc* coherent twin boundary considered above ($\mathbf{U} = (1, 1, 1)/3$ and $\mathbf{n} = (1, 1, 1)/\sqrt{3}$), with the symmetry operation $\mathbf{S} = (0, 0, -1)$ representing 90° rotation about $[00\bar{1}]$, the product

$\mathbf{U} \circ \mathbf{S} = (0, 1, -1)/2$ decomposes into $\mathbf{N} = \mathbf{0}$ and $\mathbf{L}_i = \mathbf{U} \circ \mathbf{S}$, i.e., the boundary is a 70.5° tilt about $[01\bar{1}]$. Thus, one concludes that this boundary has a representation with vanishing tilt component ($\lambda_F = 0$), and another with vanishing twist component ($\nu_F = 0$), i.e., it has both twist and tilt character. Generally, Fortes decomposition allows for identification of all pure-twist and pure-tilt boundaries, and the angles ν_F , λ_F may serve as quantitative measures of the twist and tilt contributions to a mixed boundary. Fig. 3 depicts the values of the parameters ν_F and λ_F for a fixed misorientation ($\Sigma 7$) and compares them to values of ν and λ . Fig. 3

Sections through the distributions of ν_F and λ_F for the $\Sigma 7$ misorientation are shown in Fig. 4. Some roughness of the distribution of the angle ν_F can be easily noticed. To give a numerical example, let us consider the decomposition of the boundary given by Fig. 4

$$\mathbf{n} = \left(\zeta, 0, \sqrt{1 - \zeta^2} \right) \quad \text{and} \quad \mathbf{U} = (\sqrt{2} - 1)\mathbf{n}, \quad (0 \leq \zeta \leq 1). \quad (4)$$

In the presence of symmetry, the angle ν_F approaches 45° as ζ approaches 0; e.g., $\nu_F \approx 44.97^\circ$ for $\zeta = 0.0003$. For $\zeta > 0$, vectors of eq.(4) represent explicitly twist boundaries, but when ζ equals 0, the boundary has also pure-tilt character and the angle ν_F of the twist component drops from nearly 45° to zero. This example shows the discontinuity of the components with respect to the macroscopic boundary parameters. With such discontinuities and lack of smoothness, the twist and tilt components cannot be reliably estimated from error-affected experimental data.

5.3 Distances in the boundary space

The next approach differs conceptually from the boundary decomposition but it has been used for extracting information similar to that expected from the decomposition [18, 19]. The deviation of a boundary from the nearest pure-twist and pure-tilt boundaries can be quantitatively described using a distance in the grain boundary parameter space. The distance must involve both misorientations and planes and account for equivalent boundary representations [12, 20]. Here we use the same metric function as in [19]: the distance between two boundaries equals to $\min \left(\sqrt{\Phi^2 + (\phi_1^2 + \phi_2^2)/2} \right)$, where Φ is the angle of the rotation relating the two misorientations, ϕ_i is the angle between boundary normals given in the systems of the i -th grain, and the minimization is over all symmetrically equivalent boundary representations¹. Clearly, close boundaries separated by small distances have similar macroscopic boundary parameters (and vice versa). The distances of a given boundary to the nearest pure-twist and the nearest pure-tilt boundaries are denoted by δ_N and δ_L ,

¹One could define analogous distances based on disorientations, but such parameters would not bring in anything new to our considerations. Therefore, and for brevity, we admit only these based on *all* equivalent boundary representations.

respectively. In particular, $\delta_N = 0^\circ$ for pure twists, and $\delta_L = 0^\circ$ for pure-tilt boundaries. Example sections through the distributions of these parameters are shown in Fig. 5. Fig. 5

The distances δ_L to the nearest pure-tilt take the value of zero for the same boundaries as the angles ν_F of twist components. Similarly, δ_N and λ_F vanish at the same locations in the boundary space. Hence, δ_L and δ_N are expected to be correlated to ν_F and λ_F , respectively. This is true for the distances δ_N and the angles λ_F , but the correlation between ν_F and δ_L turns out to be relatively poor (Fig. 6). Although λ_F and ν_F are just rotation angles, Fig. 6 whereas distances δ_N and δ_L involve both rotation angles and angles between boundary normals, still the angles of components are frequently larger than the corresponding distances. The maximal values of the considered parameters are

$$\max(\nu_F) \approx 45^\circ, \max(\lambda_F) \approx 54.7^\circ \quad \text{and} \quad \max(\delta_L) \approx 7.4^\circ, \max(\delta_N) \approx 28.3^\circ; \quad (5)$$

the data for δ_N and δ_L are cited after [19], the largest ν_F corresponds to the case described above by eq.(4), and the largest λ_F is obtained by decomposition of $\mathbf{U} = (0, 1, 1)/(1 + \sqrt{3})$ with respect to $\mathbf{n} = (1, 0, 0)$.

The parameters δ_N and δ_L have a significant disadvantage: calculating them for a given boundary is cumbersome. In practice, determining the nearest pure-twists and pure-tilts requires application of optimization techniques. Consequently, computation times for large boundary data sets become long. With the implementation used here [21], the time needed for computing both δ_N and δ_L for 10^4 boundary segments on a personal computer was about 30 minutes.

5.4 "Tilt/twist component (TTC)" parameter

Finally, let us consider an even simpler approach to quantification of twist and tilt contributions. It is linked directly to the equation defining tilt and twist boundaries ($|\mathbf{n} \cdot \mathbf{u}| = 0, 1$). Concretely, the contribution of the twist and tilt components is measured by the parameter $|\mathbf{n} \cdot \mathbf{u}|$; see [23]. Equivalently, besides $|\mathbf{n} \cdot \mathbf{u}|$, the angle α between directions of \mathbf{n} and \mathbf{u} is used [16]. In [24], the parameter $|\mathbf{n} \cdot \mathbf{u}|$ is referred to as TTC, and we will use this designation also to α . Clearly, the TTC parameter is independent of the misorientation-angle. Since $|\mathbf{n} \cdot \mathbf{u}|$ can be expressed via \mathbf{N}^2 and \mathbf{L}_i^2 , the single TTC parameter is less informative than the complete twist and tilt components, or than the pairs of twist and tilt angles ν and λ .

The TTC parameter is also affected by crystal symmetries: although is not influenced by the grain exchange nor by the choice of the sense of \mathbf{n} , it still takes a number of values. As in [16, 23–25], vectors \mathbf{u} and \mathbf{n} corresponding to a disorientation can be used, and this leads to unique $|\mathbf{n} \cdot \mathbf{u}|$ and α . However, for large angle boundaries, there are no clear reasons for ignoring other boundary representations, and using only disorientations has the drawbacks of the approach described in subsection 5.1.

Similarly as in Fortes decomposition, one may also eliminate the ambiguity by choosing the axes leading to either minimal or maximal values of $|\mathbf{n} \cdot \mathbf{u}|$ or α . Such parameters have not been used before. Although interpretation of the extremal values $\alpha_N = \min(\alpha)$ and $\alpha_L = 90^\circ - \max(\alpha)$ of α differs from that of the distances δ_N and δ_L , these pairs turn out to be close. Numerical tests for the cubic case indicate that $\alpha_N \geq \delta_N$ and $\alpha_L \geq \delta_L$. Moreover, α_L and α_N are not larger than about 10° and 29° , respectively; cf. eq.(5). The distributions of α_L and α_N resemble those of δ_L and δ_N (Fig. 7). More generally, the parameters α_L and α_N are strongly correlated to δ_L and δ_N , respectively. These correlations are demonstrated in Fig. 8.

Fig. 7

Fig. 8

Based on the closeness of the pairs (α_L, α_N) and (δ_L, δ_N) , statistical results obtained from experimental data using α_L and α_N are expected to be similar to corresponding results based on δ_L and δ_N . On the other hand, the former are easier to compute than the latter: the code is simpler, and the running time was about 10^3 times shorter.

5.5 Discrimination of near-tilt boundaries

The above shows a number of ways to characterize mixed boundaries. The considered parameters are summarized in Tab. 1. The applicability of these quantities as measures of mixed boundary geometry depends on objectives and circumstances of a particular analysis. Because of their instability, the angles ν_F are not suitable for checking data affected by even very small perturbations. This makes ν_F inapplicable to examination of experimental boundary data. Moreover, small maxima of the parameters δ_L and α_L as well as Figs. 5 and 7 indicate that deviations from pure-tilt boundaries are generally small compared to remaining parameters. It is worth adding that in the random case, the mean value of δ_L is only 1.6° , and about 84% of boundaries deviate from pure-tilt by $\delta_L \leq 3^\circ$ [19]. These numbers suggest that with cubic crystal symmetry, for boundaries to be reliably classified as near-tilt, a relatively high experimental accuracy (1° or better) would be needed.

Tab. 1

As the maximal distance to the nearest pure-twist boundary is quite large, and mean distance is 11.8° [19], the accuracy required for classification of near-twist boundaries is considerably lower. One may ask about the origin of this asymmetry between near-tilt and near-twist boundaries. Although the formal conditions for the twist and tilt boundaries look similar ($|\mathbf{n} \cdot \mathbf{u}| = 1$ and 0 , respectively), they determine very different entities in the boundary space: twist boundaries are associated with three degrees of freedom whereas tilt boundaries with four degrees. Therefore, the distributions of these boundary types in the parameter space are different.

6. Analysis of mixed boundaries in a nickel-based alloy

To illustrate the above considerations, we analyzed the boundary data set "Small IN100"

of fine-grained nickel-based superalloy IN100 acquired by M.A.Groerber using 3D-EBSD. The reference [26] provides details of the material processing history and a full description of the method of data acquisition. The grain boundary distribution (GBD) in the space of macroscopic boundary parameters and grain boundary energy as a function of these parameters for a superset of "Small IN100" are discussed in [27].

Our processing of the data consisted of reconstruction and meshing of the boundary network (carried out using DREAM.3D [28]), simplification of the mesh (by QSLIM 2.0 [29]), and calculation of various boundary distributions (carried out using in-house software). The reconstructed set contained 1853 grains. The total number of boundary segments was about 3.5×10^5 . For illustration, a fragment of the investigated boundary network with the actual mesh is shown in Fig. 9. Example sections through GBD are shown in Fig. 10. They are similar to corresponding figures of [27]. The ubiquity of coherent twins visible in microstructure images [26] is reflected by a very high peak at the $\Sigma 3$ misorientation and (111) plane.

Fig. 9

Fig. 10

The simplest way to evaluate the frequencies of occurrence of near-tilt and near-twist boundaries is to calculate the distributions of the parameters listed in Tab. 1. Potential peaks at zero would indicate presence of the boundaries of a given type. The distributions were strongly affected by the high frequency of twins. In order to examine the impact of the twins, distributions were also calculated for boundaries differing from $\Sigma 3$ by more than 2° . In this smaller set, the number of boundary segments was nearly 2.8×10^5 .

Let us start with the familiar distribution of disorientation angles – the most basic of one-dimensional projection of GBD (Fig. 11). It has a very strong peak at 60° , the result consistent with the presence of twins. Because of experimental errors and data processing methods, only points at the high-end ($7^\circ \leq \theta \leq 15^\circ$) of low-angle boundaries are reliable, and the boundaries in this range are overrepresented. Besides that, the distribution is relatively flat. For illustration, the disorientation angle distribution is presented in two forms; all remaining distributions are shown only as multiples of corresponding random distributions. The latter were obtained numerically by generating at least 10^6 random boundaries.

Fig. 11

The distributions of the angles λ and ν of components of disorientations and of the TTC parameter α are shown in Fig. 12. In terms of the locations of peaks, they clearly reflect the partial information contained in Fig. 10. The distributions of λ and ν are dominated by the (111) twists, in particular, by the coherent twin. The peak at $\alpha = 0^\circ$ has the same origin. For α exceeding 25° , the distribution becomes uniform, i.e., close to the random case; the latter observation applies also to $\alpha = 90^\circ$ corresponding to tilts in the domain of disorientations. Thus, the distribution of α , and also that of ν , show the absence of near-tilt boundaries in the representations with the smallest misorientation angles.

Fig. 12

The distributions of the smallest tilt angle λ_F , the distance to the nearest pure-twist

boundary δ_N , and the minimal TTC parameter α_N , are shown in Fig. 13. As one could expect, there is not much difference in shapes of these functions. Let us focus on the graph for δ_N . Elevated values near $\delta_N = 0^\circ$ indicate that twist boundaries are overrepresented. This is also true for the data without $\Sigma 3$ boundaries, but the values are lower than in the case of the complete data set. The width of the peak at $\delta_N = 0^\circ$ is relatively large; based on Figs. 10 and 12, it spreads beyond $\delta_N \approx 10^\circ$. Then, there is a minimum at δ_N near $21 - 23^\circ$. These low values of the distribution for larger δ_N are attributed to the balance requirement: if some data (near $\delta_N = 0^\circ$) are above 1, there must be data below 1. This is confirmed by the fact that the minimum becomes shallow when $\Sigma 3$ boundaries are removed and the maximum at $\delta_N = 0^\circ$ diminishes. The results at the far end of the abscissa are affected by large errors because of low probability of occurrence of such boundaries. *Fig. 13*

It remains to consider the population of near-tilt boundaries. The parameter ν_F , as not stable with respect to perturbations of input data, must be excluded. The distributions of δ_L and α_L are shown in Fig. 14. Their reliability is low because of low resolution of the investigated data. Moreover, as the probability of occurrence of boundaries strongly decreases with growing δ_L and α_L [19], so does the reliability of the distributions. For the complete data set, the values of the distributions at the most reliable points near $\delta_L = 0^\circ = \alpha_L$ slightly exceed 1. This means that the tilt boundaries are overrepresented. The elevation is attributed to the twin boundaries. For the set without $\Sigma 3$ boundaries, the distributions at zero are practically the same as in the random case. *Fig. 14*

Let us note that the one-dimensional distributions of Figs. 13 and 14 are complicated projections of GBD. Such figures might summarize information on near-twist boundaries scattered in the complete GBD. In the considered case, however, the figures do not really provide any new facts beyond those easily deductible from the GBD. However, there is no ground for expecting that this is generally true. The analyzed GBD is very simple: most of its parts are close to random, and the only elevated values are these near (111) twists with a very strong peak at the coherent twin boundary. Without such a dominating maximum, and with higher experimental resolution and larger data sets, more detailed features of GBDs may be revealed. In these cases, the functions depicting frequencies of near-tilt and near-twist boundaries may provide information not apparent on GBDs.

7. Conclusions

Possible ways of analyzing mixed large-angle boundaries have been scrutinized. In the simplest classification, the considered methods are either based on the boundary decomposition into twist and tilt components or on other measures of deviations from pure-twist or tilt boundaries. Furthermore, they are either limited to disorientations or take into account all symmetrically equivalent boundary representations.

The simplistic approaches limited to disorientations and ignoring other symmetrically equivalent boundary representations (with parameters ν , λ and α) provide only partial information about geometry of boundaries. Boundary characterization by these methods is inconsistent with the definitions of twist and tilt boundaries based on the requirement of existence of relationships between misorientation axis and the boundary plane (as the existence cannot be detected without examining all symmetrically equivalent boundary representations). In consequence, the approaches limited to disorientations are not suitable for comprehensive studies of boundary geometry.

Closeness of a boundary to the twist or tilt geometries can be detected only by taking into account all its representations. We analyzed three different sets of parameters as possible measures of this closeness:

- the smallest angles (ν_F , λ_F) of boundary components obtained using Fortes decomposition,
- properly defined distances to pure-twist or tilt boundaries (δ_L , δ_N), and
- the newly introduced parameters (α_L , α_N) defined as the extreme values of the angle between the misorientation axis and the normal to the boundary plane.

The applicability of the Fortes decomposition and (ν_F , λ_F) parameters to analysis of boundaries is shown to be limited. It can be used for identification of ideal twist or tilt boundaries, but it is not suitable for analysis of error-affected data because of instability of one of the angles (ν_F) to small perturbations of input data.

Consequently, the choice of approaches to experimental grain boundary data is confined to the distances to pure-twist or pure-tilt boundaries (δ_L , δ_N) and extreme values of the angle between the misorientation axis and the normal to the boundary plane (α_L , α_N). Detailed analyzes show that the distances (δ_L , δ_N) are strongly correlated with the angles (α_L , α_N) and as such, the pairs are expected to lead to similar conclusions. However, computing the angles is considerably easier than getting the distances.

On the experimental side, as the deviations of boundaries from pure-tilt boundaries (δ_L and α_L) are relatively small (a couple of degrees), in order to discriminate near-tilt boundaries high accuracy data are needed.

Acknowledgments

The authors are grateful to M.A. Groeber of U.S. Air Force Research Laboratory for permission to use the "Small IN100" grain boundary data set. Work of K.G. was supported by the European Union under the European Social Fund within Project No. POKL.04.01.00-00-004/10.

References

- [1] Sutton AP, Balluffi RW. Interfaces in crystalline materials. Oxford: Clarendon Press; 1995.
- [2] Goux C. Can Metall Quart 1974;13:9.
- [3] Rohrer GS, Saylor DM, El Dasher B, Adams BL, Rollett AD, Wynblatt P. Z Metallkd 2004;95:197.
- [4] Lienert U, Li SF, Hefferan CM, Lind J, Suter RM, Bernier JV, Barton NR, Brandes MC, Mills MJ, Miller MP, Jakobsen B, Pantleon W. JOM-J Min Met Mat S 2011;63:70.
- [5] Tafuri F, Miletto Granozio F, Carillo F, Di Chiara A, Verbist K, Van Tendeloo G. Phys Rev B 1999;59:11523.
- [6] Hardouin Duparc OBM, Couzinié JP, Thibault-Pénisson J, Lartigue-Korinek S, Décamps B, Priester L. Acta Mater 2007;55:1791.
- [7] Randle V. The measurement of grain boundary geometry. London: Taylor & Francis; 1993.
- [8] Lange FF. Acta Metall 1967;15:311.
- [9] Fortes MA. Acta Cryst A 1973;29:68.
- [10] Glowinski K. Solid St Phen 2013;203-204:427.
- [11] Morawiec A. Orientations and rotations: Computations in crystallographic textures. Berlin: Springer; 2004.
- [12] Morawiec A. J Appl Cryst 2009;42:783.
- [13] Warrington DH, Bufalini P. Scripta Metall 1971;5:771.
- [14] Pospiech J, Sztwiertnia K, Haessner F. Textures Microstruct 1986;6:1986.
- [15] Morawiec A. Acta Cryst A 1997;53:273.
- [16] Rowenhorst DJ, Voorhees PW. Metall Mater Trans A 2005;36:2127.
- [17] Morawiec A. J Appl Cryst 2009;42:308.
- [18] Morawiec A. J Appl Cryst 2011;4:1152.
- [19] Morawiec A. Scripta Mater 2009;61:438.

- [20] Cahn JW, Taylor JE. *J Mater Sci* 2006;41:7669.
- [21] Glowinski K, Morawiec A., in: *Proc 1st Int Conf 3D Mater Sci*, p. 119. De Graef M, Poulsen HF, Lewis A, Simmons J, Spanos G (Eds.). Wiley; 2012.
- [22] Beladi H, Rohrer GS. *Metall Mater Trans A* 2013;44:115.
- [23] Seidman DN. Experimental investigation of internal interfaces in solids, in: Wolf D, Yip DS (Eds.). *Materials interfaces, atomic-level structure and properties*. London: Chapman & Hall; 1992.
- [24] Amouyal Y, Rabkin E, Mishin Y. *Acta Mater* 2005;53:3795.
- [25] Krakauer BW, Seidman DN. *Acta Mater* 1998;46:6145.
- [26] Groeber MA, Haley BK, Uchic MD, Dimiduk DM, Ghosh S. *Mater Charact* 2006;57:259.
- [27] Rohrer GS, Li J, Lee S, Rollett AD, Groeber M, Uchic MD. *Mater Sci Tech* 2010;26:661.
- [28] <http://dream3d.bluequartz.net/index.html>
- [29] Garland M, Heckbert P. *Proc. SIGGRAPH'97*, p. 209. New York: ACM Press; 1997.

Appendix

The derivations of the relationships listed in section 3 are sketched below for the sake of completeness.

1. With a finite non-zero Rodrigues vector \mathbf{U} and a unit vector \mathbf{n} , the twist \mathbf{N} about \mathbf{n} and tilt \mathbf{L}_1 about an axis perpendicular to \mathbf{n} satisfying $\mathbf{U} = \mathbf{N} \circ \mathbf{L}_1$ are given by eqs.(1).

Let x be the factor relating \mathbf{N} to \mathbf{n} , i.e., $\mathbf{N} = x\mathbf{n}$. Based on $\mathbf{N} \cdot \mathbf{L}_1 = 0$ and the formula for composition of rotations one gets $\mathbf{U} \cdot \mathbf{n} = (\mathbf{N} \circ \mathbf{L}_1) \cdot \mathbf{n} = (\mathbf{N} + \mathbf{L}_1 - \mathbf{N} \times \mathbf{L}_1) \cdot \mathbf{n} = \mathbf{N} \cdot \mathbf{n} = x$. Hence, one has $\mathbf{N} = (\mathbf{U} \cdot \mathbf{n})\mathbf{n}$ and $\mathbf{L}_1 = (-\mathbf{N}) \circ \mathbf{U} = -(\mathbf{U} \cdot \mathbf{n})\mathbf{n} \circ \mathbf{U}$. Eqs.(2) are obtained in analogous way.

2. The vectors \mathbf{L}_1 and \mathbf{L}_2 have equal magnitudes.

The vector $\mathbf{L}_2 = \mathbf{L}_2 \circ \mathbf{N} \circ (-\mathbf{N}) = \mathbf{N} \circ \mathbf{L}_1 \circ (-\mathbf{N})$ is obtained by rotating \mathbf{L}_1 by \mathbf{N} , and hence, the magnitudes of \mathbf{L}_1 and \mathbf{L}_2 are equal.

3. If $\mathbf{L}_1 = \mathbf{L}_2$, then either $\mathbf{N} = \mathbf{0}$ or $\mathbf{L}_i = \mathbf{0}$.

Based on $\mathbf{N} \cdot \mathbf{L}_i = 0$, the equality $\mathbf{N} \circ \mathbf{L}_1 = \mathbf{L}_2 \circ \mathbf{N} = \mathbf{L}_1 \circ \mathbf{N}$ takes the form $\mathbf{N} + \mathbf{L}_1 - \mathbf{N} \times \mathbf{L}_1 = \mathbf{N} + \mathbf{L}_1 - \mathbf{L}_1 \times \mathbf{N}$ or $\mathbf{N} \times \mathbf{L}_1 = \mathbf{0}$. The equalities $\mathbf{N} \times \mathbf{L}_1 = \mathbf{0}$ and $\mathbf{N} \cdot \mathbf{L}_1 = 0$ together with $\mathbf{N} \circ \mathbf{L}_1 \neq \mathbf{0}$ implicate that either \mathbf{N} or \mathbf{L}_1 must be equal to $\mathbf{0}$. Analogous statement applies to \mathbf{L}_2 .

4. The magnitudes of \mathbf{U} , \mathbf{N} and \mathbf{L}_i are related by eq.(3).

From $\mathbf{U} = \mathbf{N} \circ \mathbf{L}_1$ and $\mathbf{N} \cdot \mathbf{L}_1 = 0$ follows $1 + \mathbf{U}^2 = 1 + (\mathbf{N} + \mathbf{L}_1 - \mathbf{N} \times \mathbf{L}_1)^2 = 1 + \mathbf{N}^2 + \mathbf{L}_1^2 + \mathbf{N}^2 \mathbf{L}_1^2 = (1 + \mathbf{N}^2)(1 + \mathbf{L}_1^2)$. Analogous steps lead to the relationship for \mathbf{L}_2 .

5. The decomposition of \mathbf{U} with respect to \mathbf{n} gives the same angles as that with respect to $(\xi\mathbf{u}) \circ \mathbf{n} \circ (-\xi\mathbf{u})$, where ξ is an arbitrary real number.

One needs to consider the decomposition of \mathbf{U} with respect to $\mathbf{n}_\xi = (\xi\mathbf{u}) \circ \mathbf{n} \circ (-\xi\mathbf{u})$ into $\mathbf{N}_\xi \circ \mathbf{L}_\xi$. The squared magnitude of the twist component $\mathbf{N}_\xi = (\mathbf{U} \cdot \mathbf{n}_\xi)\mathbf{n}_\xi$ is given by $\mathbf{N}_\xi^2 = \mathbf{U}^2 (\mathbf{u} \cdot ((\xi\mathbf{u}) \circ \mathbf{n} \circ (-\xi\mathbf{u})))^2$. A little tedious but simple calculation shows that $\mathbf{u} \cdot ((\xi\mathbf{u}) \circ \mathbf{n} \circ (-\xi\mathbf{u})) = \mathbf{u} \cdot \mathbf{n}$. Hence, $\mathbf{N}_\xi^2 = \mathbf{U}^2 (\mathbf{u} \cdot \mathbf{n})^2 = (\mathbf{U} \cdot \mathbf{n})^2 = \mathbf{N}^2$. The equality of \mathbf{N}_ξ^2 and \mathbf{N}^2 implicates the equality of corresponding twist angles. The equality of magnitudes of tilt components \mathbf{L}_ξ and \mathbf{L}_i follows from $\mathbf{N}_\xi^2 = \mathbf{N}^2$ and eq.(3). Similar calculations show that the decomposition of \mathbf{U} with respect to \mathbf{n} gives the same angles as the decomposition of $(\xi\mathbf{n}) \circ \mathbf{U} \circ (-\xi\mathbf{n})$ with respect to the same vector \mathbf{n} .

6. The tilt angle λ satisfies the inequality $\lambda \leq 2\alpha = 2 \arccos(|\mathbf{n} \cdot \mathbf{u}|)$.

From the first of eqs.(1), one has $\mathbf{N}^2/\mathbf{U}^2 = ((\mathbf{U} \cdot \mathbf{n})\mathbf{n})^2/\mathbf{U}^2 = (\mathbf{n} \cdot \mathbf{u})^2$. On the other hand, based on eq.(3), one gets $\mathbf{N}^2/\mathbf{U}^2 = \mathbf{N}^2/((1 + \mathbf{U}^2) - 1) = \mathbf{N}^2/(\mathbf{N}^2 + \mathbf{L}_i^2 + \mathbf{N}^2\mathbf{L}_i^2) = 1/(1 + \mathbf{L}_i^2 + \mathbf{L}_i^2/\mathbf{N}^2) \leq 1/(1 + \mathbf{L}_i^2)$. By combining these two relationships and using $\mathbf{L}_i^2 = \tan^2(\lambda/2)$, one obtains $\cos \alpha = |\mathbf{n} \cdot \mathbf{u}| \leq 1/\sqrt{1 + \mathbf{L}_i^2} = 1/\sqrt{1 + \tan^2(\lambda/2)} = \cos(\lambda/2)$ and $\lambda \leq 2\alpha$.

Captions

Table 1: Parameters quantifying tilt and twist contributions to a boundary. Deviations from pure-twists are listed in column (a). Column (b) contains parameters characterizing deviations from pure-tilts. Maximal values of particular parameters for cubic crystal symmetry are listed in parentheses. The symbol * marks parameters determined in the domain of disorientations.

Figure 1: Schematic of the decomposition of \mathbf{U} . The difference $\mathbf{L}_1 - \mathbf{L}_2$ (denoted by \mathbf{a}) is orthogonal to the plane containing \mathbf{U} and \mathbf{N} , i.e., $\mathbf{U} \cdot (\mathbf{L}_1 - \mathbf{L}_2) = 0 = \mathbf{N} \cdot (\mathbf{L}_1 - \mathbf{L}_2)$, whereas the sum $\mathbf{L}_1 + \mathbf{L}_2$ lies in this plane. The vectors \mathbf{b} and \mathbf{c}_i mark $\sec(\nu/2) (\mathbf{L}_1 + \mathbf{L}_2)/2$ and $\mathbf{L}_i \times \mathbf{N}$, respectively.

Figure 2: Distributions of the twist angle ν (a) and the tilt angle λ (b) for the fixed $\Sigma 7$ misorientation and variable boundary normal; cf. [22]. Stereographic projection is used.

Figure 3: Angles ν_F and λ_F of twist and tilt components for $\Sigma 7$ and two sets of random boundary planes: 10^6 planes showing the domain (gray) plus extra 10^3 planes to illustrate the density (black). The arc marks points with coordinates ν and λ obtained by decomposition of a corresponding disorientation.

Figure 4: Distributions of the smallest twist angle ν_F (a) and the smallest tilt angle λ_F (b) for $\Sigma 7$. The white circle in (a) marks one of the areas with high values of ν_F crossed by thin lines with $\nu_F = 0^\circ$. (The direction of the rotation axis is opposite to the one used in Fig. 2 of [17].)

Figure 5: Distributions of distances δ_L and δ_N to the nearest pure-tilt (a) and to the nearest pure-twist (b) boundaries for $\Sigma 7$.

Figure 6: The angles of Fortes decomposition and distances to nearest tilt or twist boundaries for 10^6 randomly generated boundaries (gray points). Black points represent boundaries for low- Σ ($\Sigma 3 - \Sigma 9$) misorientations and low-index (absolute value ≤ 4) planes. Figures illustrate the pairs ν_F and δ_L (a), λ_F and δ_N (b). The symbol ρ denotes the Spearman's rank correlation coefficient for the random data.

Figure 7: Distributions of the TTC parameter α (a) and the parameters $\alpha_L = \min(90^\circ - \alpha)$ (b) and $\alpha_N = \min(\alpha)$ (c) for $\Sigma 7$.

Figure 8: The angles α_L versus δ_L (a), and α_N versus δ_N for 10^6 randomly generated boundaries (gray points). Black points represent boundaries for low- Σ ($\Sigma 3 - \Sigma 9$) misorientations and low-index (absolute value ≤ 4) planes. In (a), boundaries between the continuous lines with $\delta_L \leq \alpha_L \leq 1.3 \delta_L$ constitute 91.2% of all boundaries. In (b), boundaries between the continuous lines with $\delta_N \leq \alpha_N \leq 1.3 \delta_N$ constitute 92.3% of all boundaries. As above, ρ is

the Spearman's rank correlation coefficient for the random data.

Figure 9: A fragment of the boundary network of the investigated Ni-based alloy. In (a), different colors represent different grain orientations. In (b), different colors represent different boundaries. The figure illustrates the mesh used for modeling the boundaries.

Figure 10: Sections through grain boundary distribution of the analyzed Ni-based alloy for $\Sigma 3$ (a) and $\Sigma 7$ (b). They are similar to corresponding figures published in [27]. The GDB was obtained in discrete form for individual equivolume bins in the space parametrized by Euler angles (misorientations) and spherical angles (normals to boundary planes). As in [27], 11 bins per 90° were used to get (a) and 9 bins per 90° to get (b).

Figure 11: (a) Conventional form of the distribution of the disorientation angle for the analyzed Ni-based alloy. Continuous line represents Mackenzie (random) distribution. (b) The same distribution as in (a), but shown as multiple of the random distribution. Because of data processing, only the points on the right side of the dashed line are reliable. In this and the remaining figures, the bin size is equal to the inverse of density of displayed points.

Figure 12: Distributions of disorientation-based parameters λ (a) ν (b) and α (c) for the investigated alloy. Disks represent results obtained from the complete data set, and crosses correspond to the data without $\Sigma 3$ boundaries.

Figure 13: Distribution of the smallest angle of tilt component λ_F (a), distribution of the distance δ_N to the nearest pure-twist boundary (b) and distribution of α_N (c) for IN100. Disks represent results obtained from the complete data set, and crosses correspond to the data without $\Sigma 3$ boundaries.

Figure 14: Distribution of the distance δ_L to the nearest pure-tilt boundary (a) and distribution of α_L (b) for IN100. Disks represent results obtained from the complete data set, and crosses correspond to the data without $\Sigma 3$ boundaries. Because of the shape of the random distribution, the larger value on the abscissa the larger errors of the presented result. This is illustrated by the error bars. Relative lengths of the bars represent only statistical errors linked to the number of counts. They do not include the errors in measuring boundary inclinations and misorientations, which are the main cause of the flattening of the distribution.

	(a)	(b)
* angles of decomposition	λ (62.8°)	ν (62.8°)
Fortes decomposition	λ_F (54.7°)	ν_F (45.0°)
distances	δ_N (28.3°)	δ_L (7.4°)
TTC-extremes	α_N (28.7°)	α_L (9.8°)
* TTC		α

Table 1:

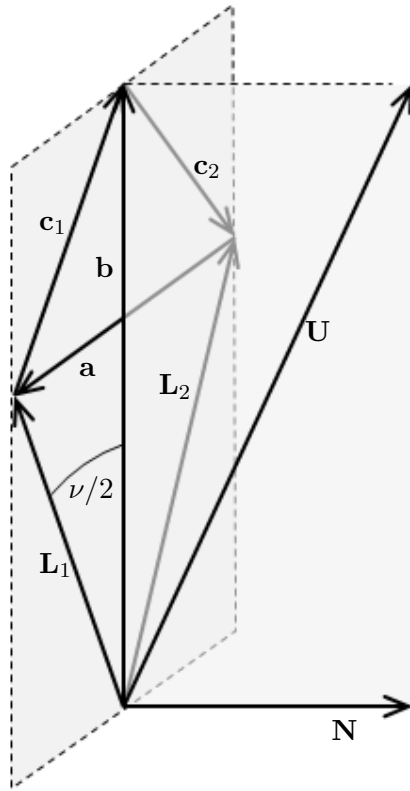


Figure 1:

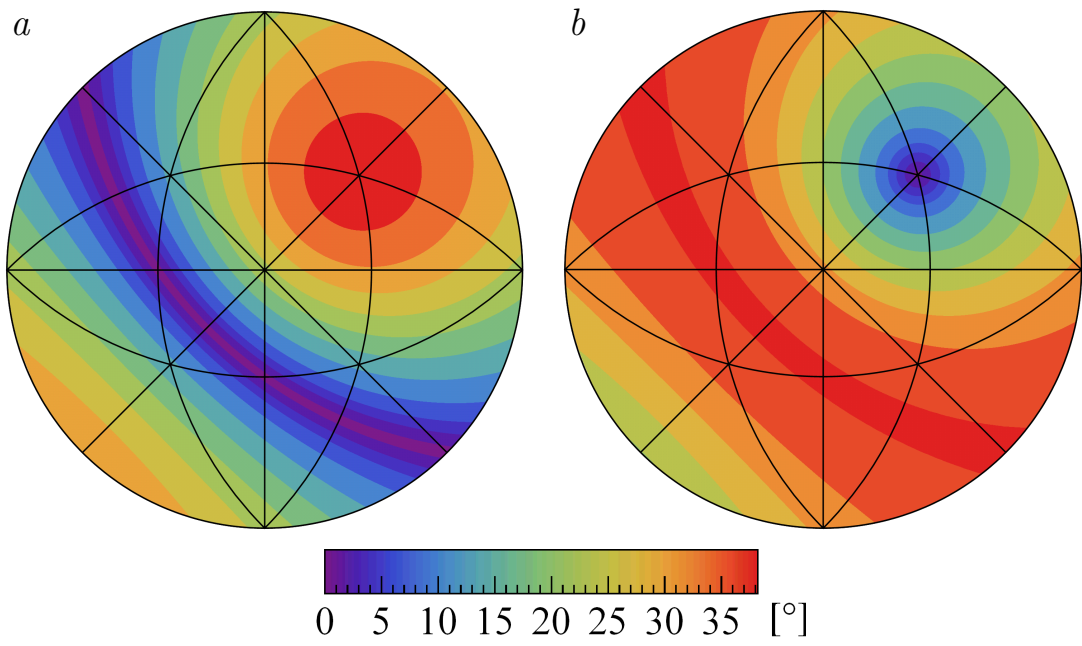


Figure 2:

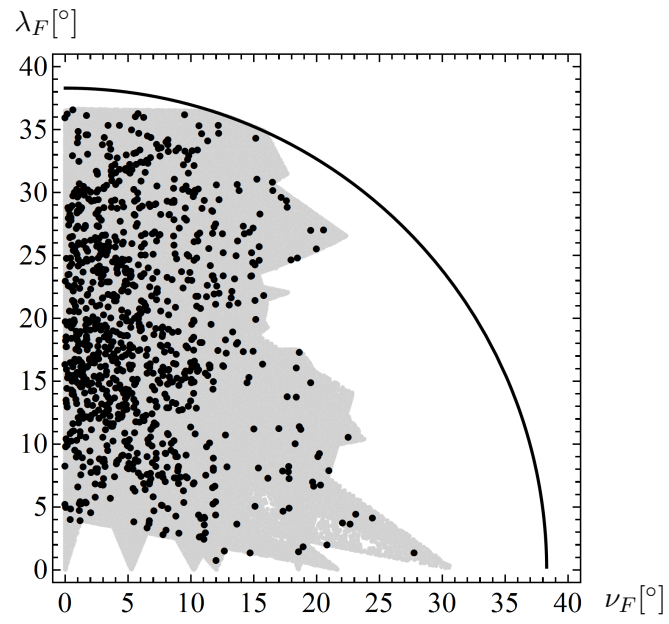


Figure 3:

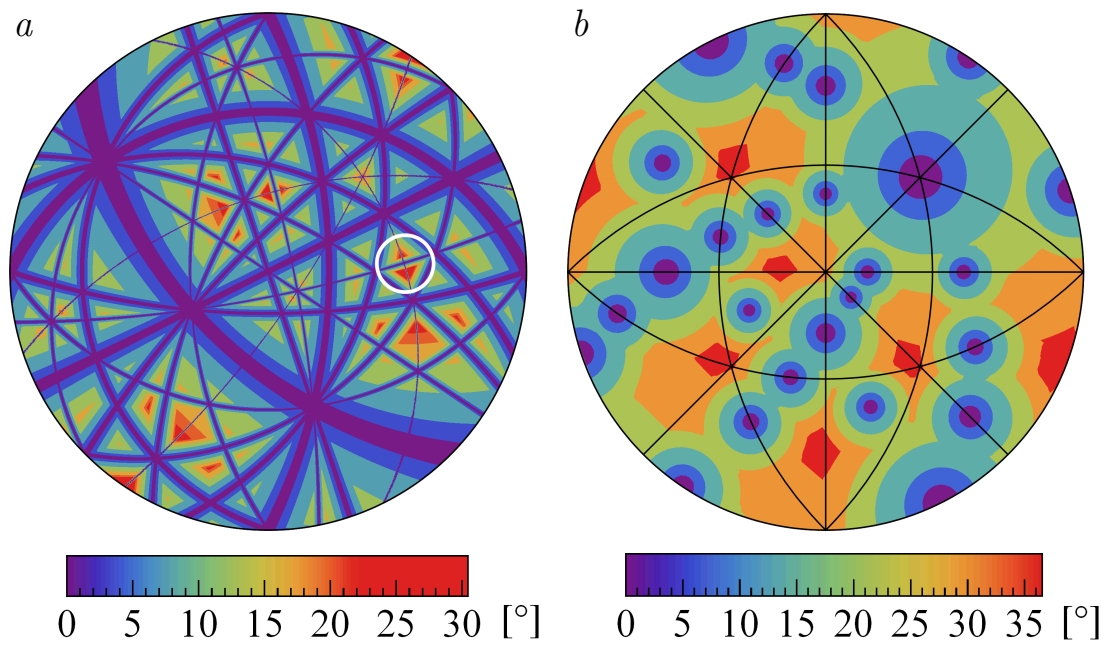


Figure 4:

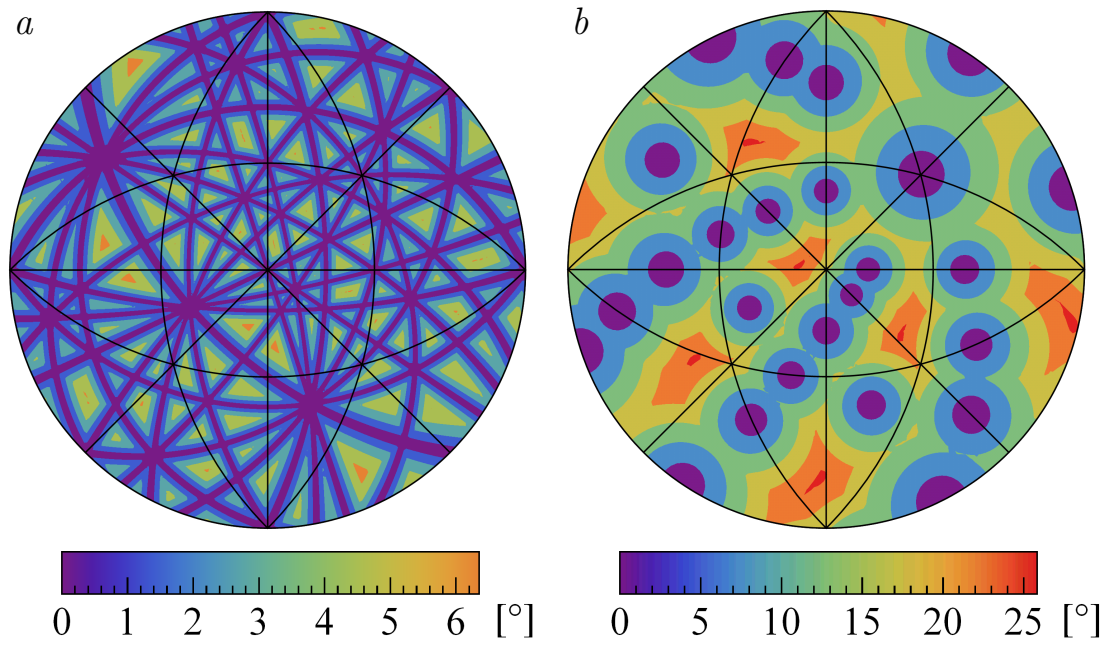


Figure 5:

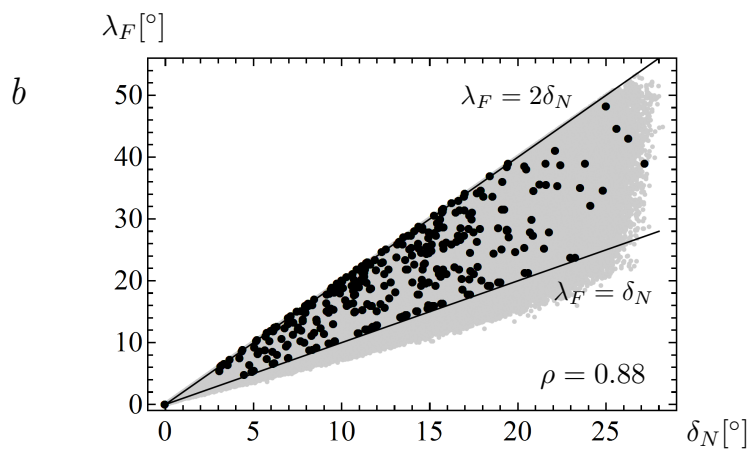
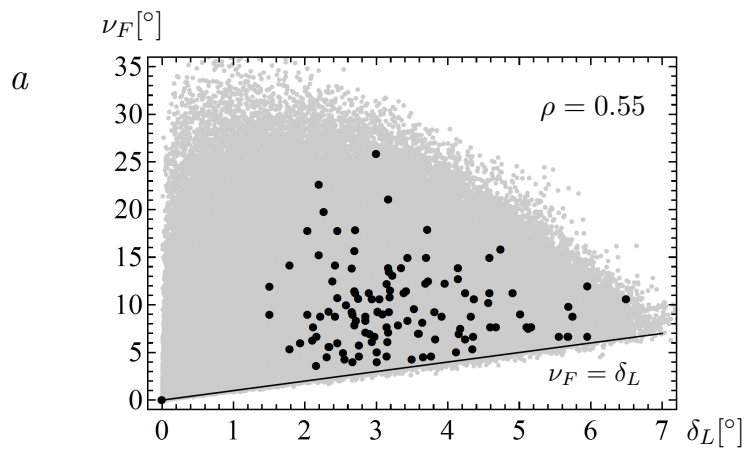


Figure 6:

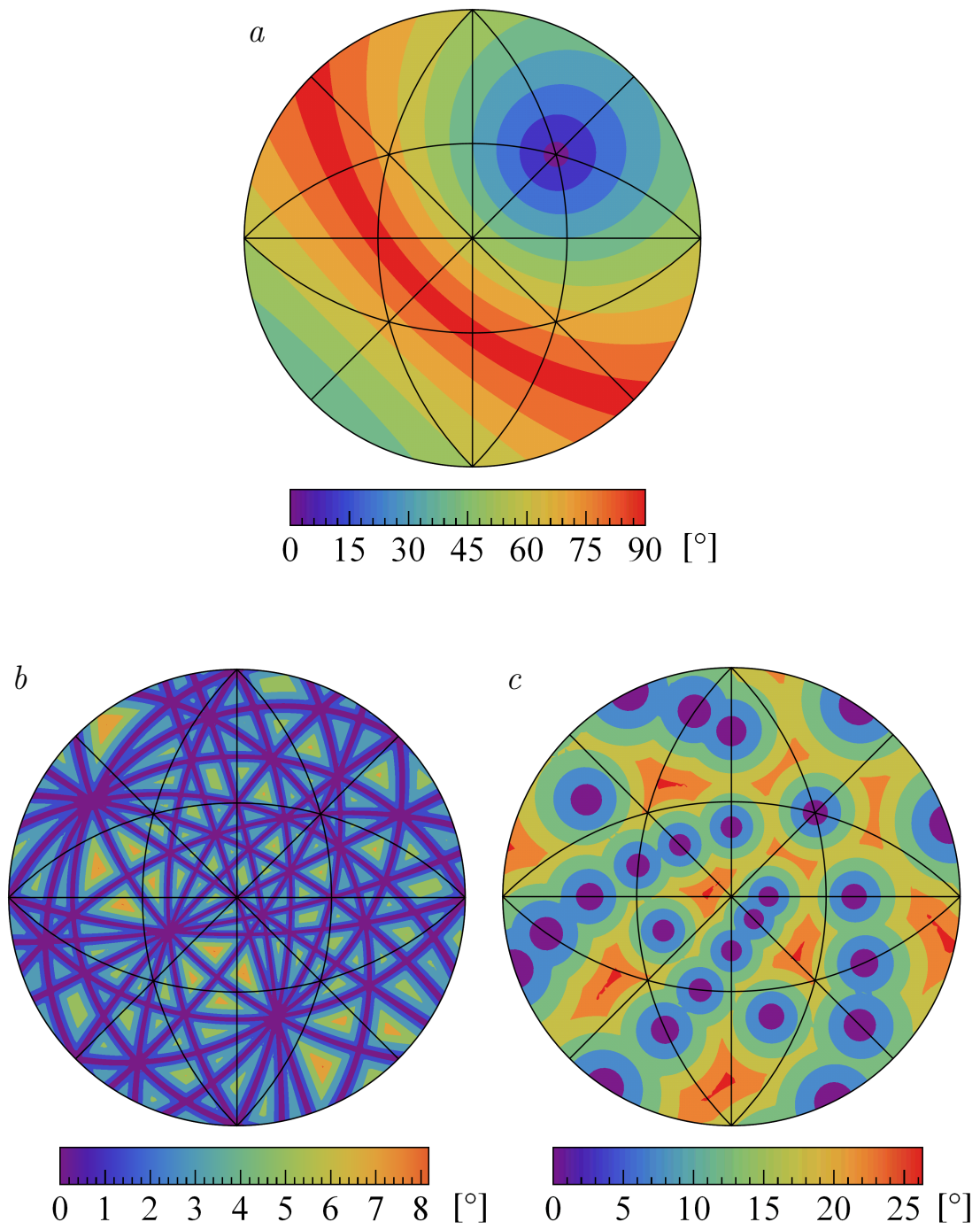


Figure 7:

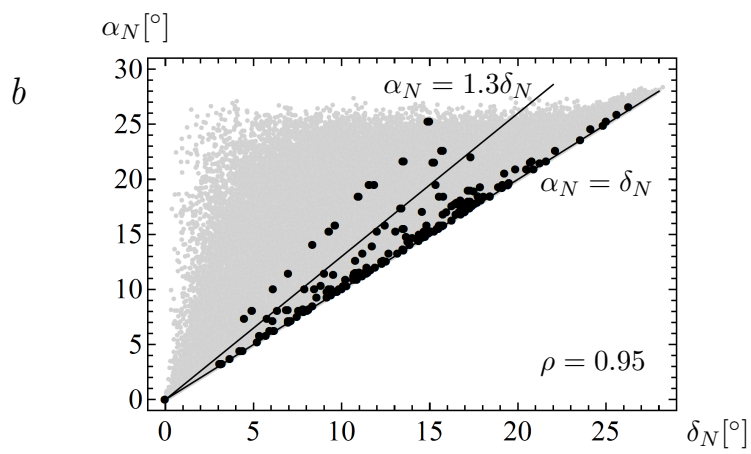
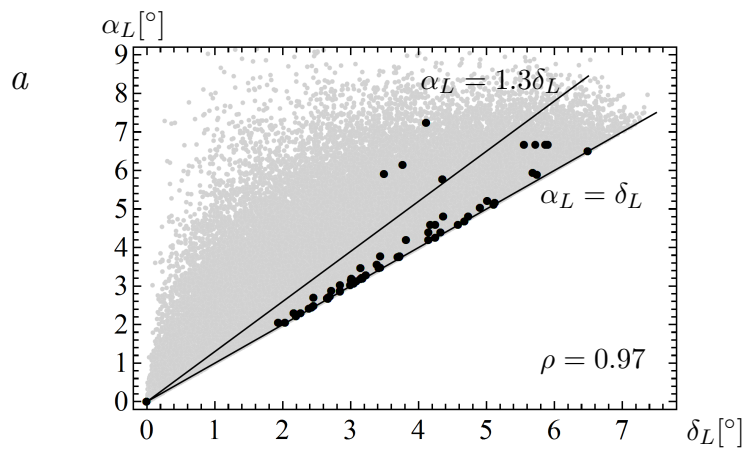


Figure 8:

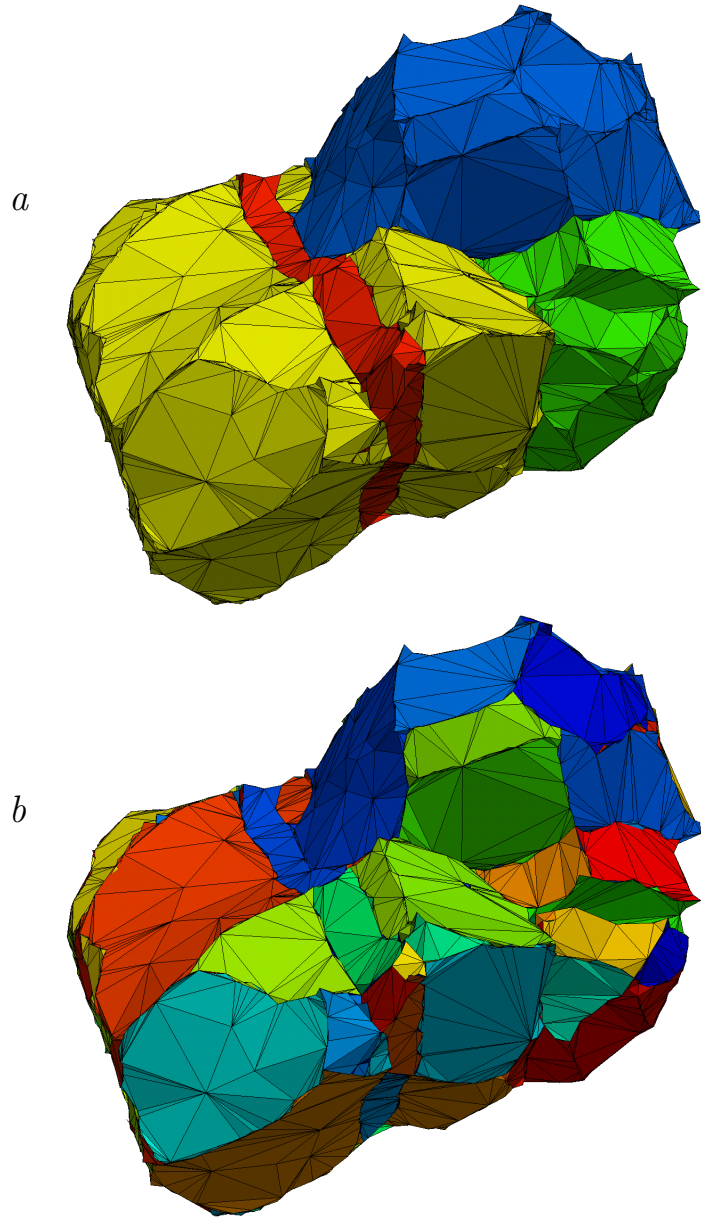


Figure 9:

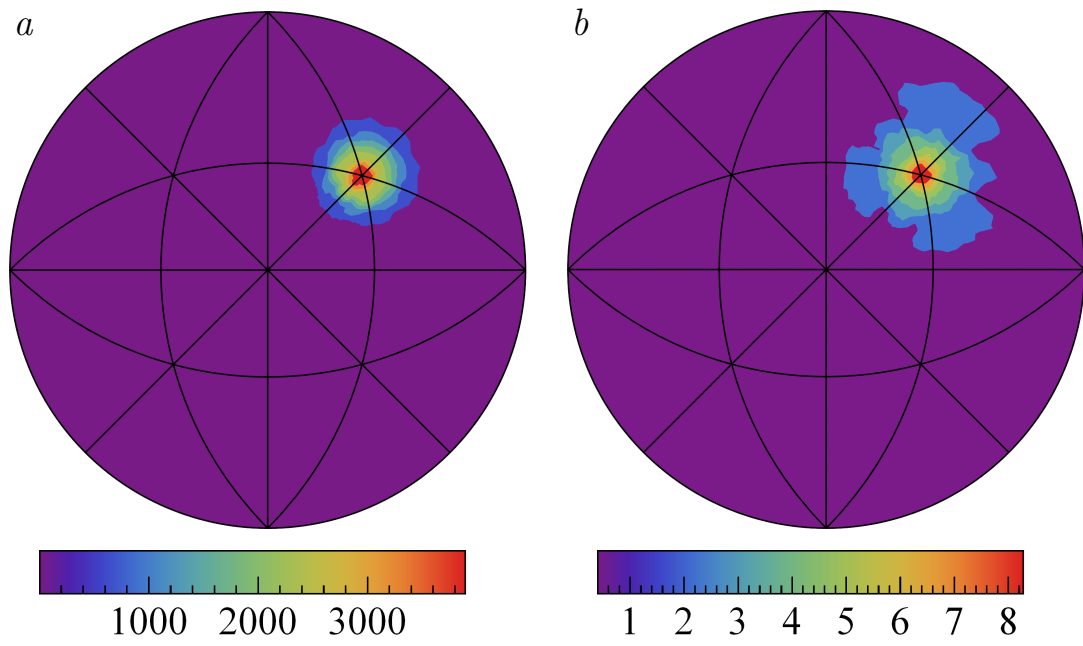


Figure 10:

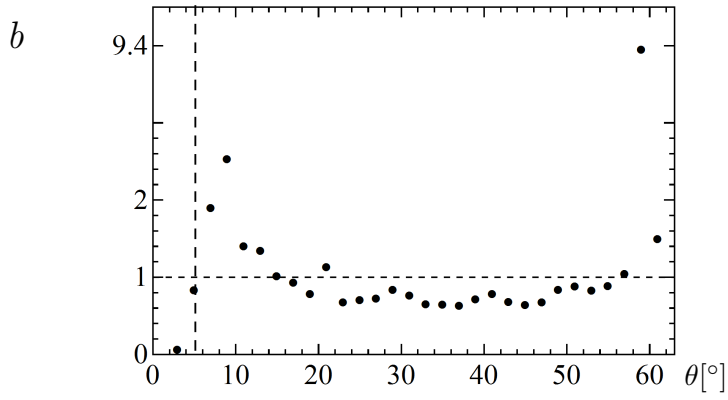
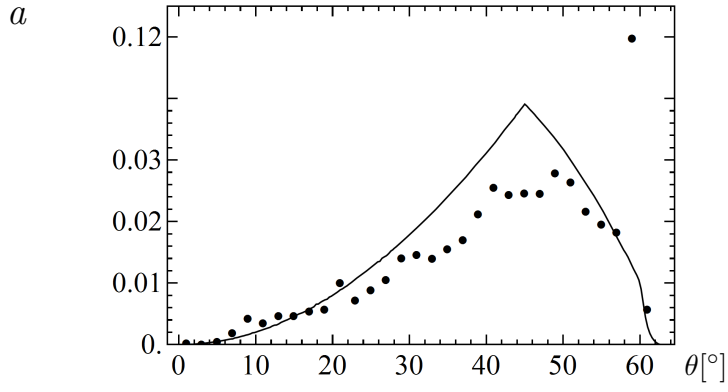


Figure 11:

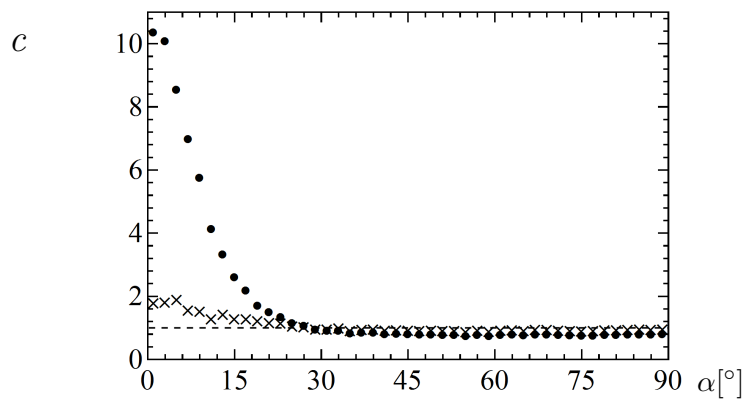
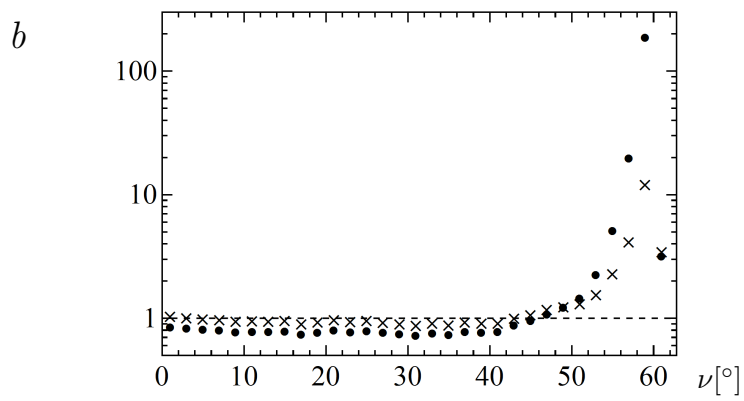
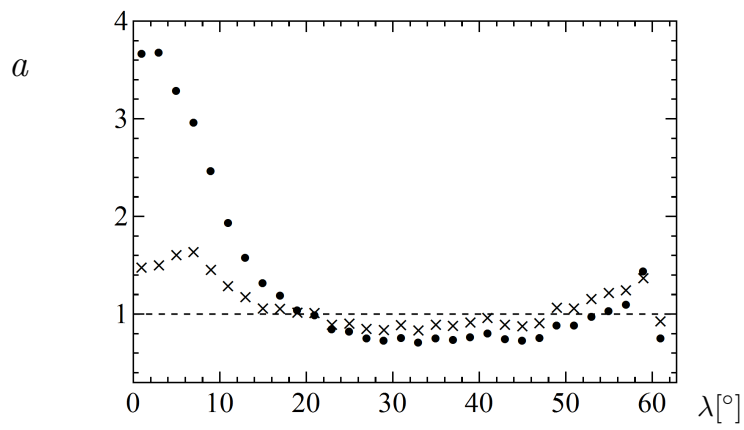


Figure 12:

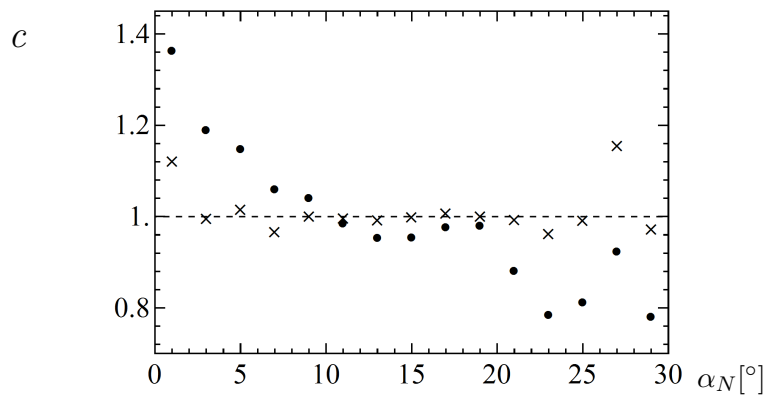
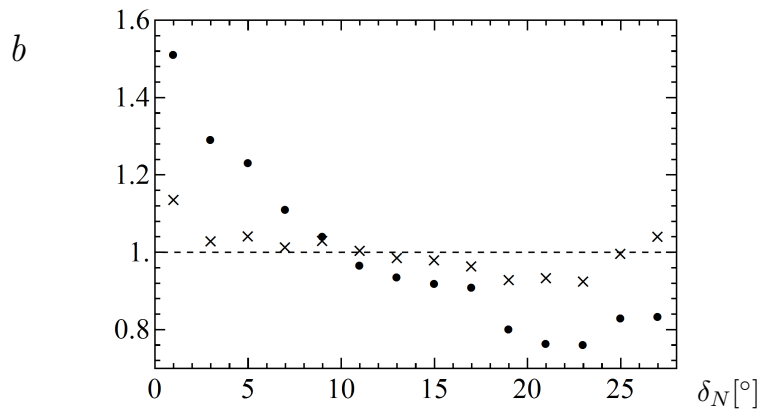
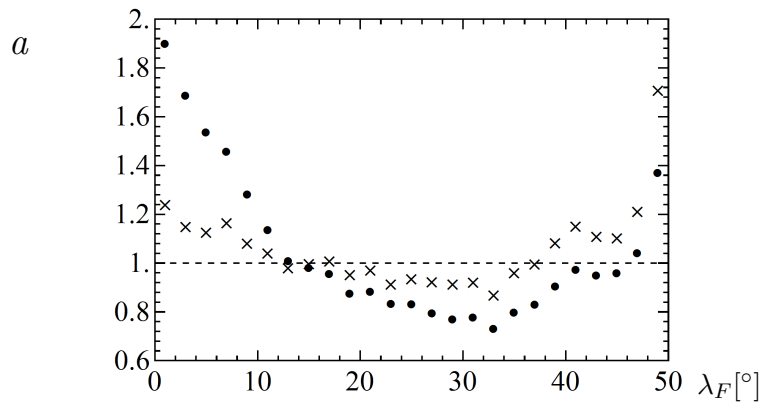


Figure 13:

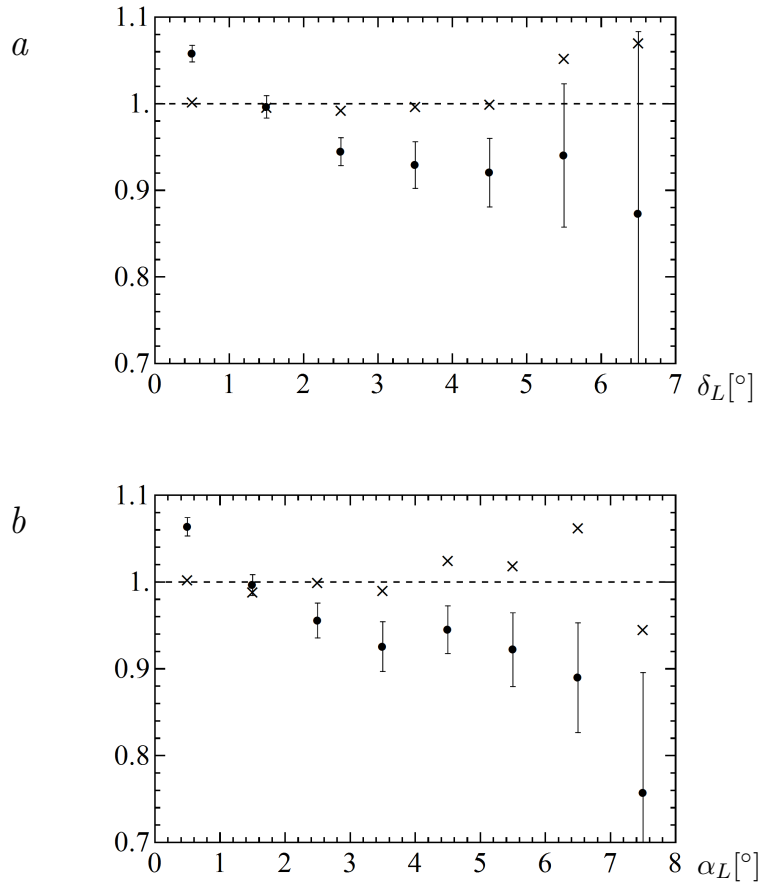


Figure 14: